Using differential satellite drag as an experiment to characterise gas–surface interactions

van der Zwaard, R.K.; Speretta, S.; Siemes, C.; Gill, E.K.A.

Important note
To cite this publication, please use the final published version (if applicable).
Please check the document version above.

ORIGINAL PAPER

Using differential satellite drag as an experiment to characterise gas–surface interactions

Rens van der Zwaard[1] · Stefano Speretta[1] · Christian Siemes[1] · Eberhard Gill[1]

Abstract

Uncertainty in atmospheric density models and drag coefficient modelling contributes to orbit prediction errors for satellites in Low Earth Orbit (LEO). It is of interest to better characterise the Gas–Surface Interactions (GSI) to improve drag coefficient modelling, which is, however, hindered by a lack of dedicated in-orbit experiments. We propose a new experiment to estimate the energy accommodation coefficient of the Diffuse Reflection with Incomplete Accommodation (DRIA) GSI model. The experiment consists of two small satellites with Global Navigation Satellite Systems (GNSS) receivers and attitude determination systems to derive atmospheric density observations from the positioning data. The experiment has two key features. The first is the satellites' close along-track formation flying, such that they should observe the same atmospheric density with a slight delay due to their along-track separation. Second, the satellites have controllable panels to modify their drag coefficients' response to GSI substantially. Hence, the satellites' atmospheric density observations will agree only when the DRIA model's energy accommodation coefficient is selected correctly. We demonstrate by simulation that the energy accommodation coefficient can be estimated at least once daily with a precision of 5–10% for satellites with decimeter-accuracy GNSS positioning. Given that GNSS receivers and attitude determination systems are common for small satellites currently in LEO, we conclude that there are plenty of opportunities to utilise existing data for the proposed experiment. Valuable byproducts would be atmospheric density observations that are relatively free of systematic errors.

1 Introduction

At orbital altitudes below approximately 600 kms, the largest source of uncertainty in trajectory predictions is errors in atmospheric drag predictions, complicating operational aspects such as collision avoidance [1]. The acceleration term acting on a spacecraft due to atmospheric drag is defined as [2]

$$\ddot{\mathbf{r}} = -\frac{1}{2} C_D \frac{A}{m} \rho v_r^2 \mathbf{e_v}, \tag{1}$$

where $\ddot{\mathbf{r}}$ is the drag acceleration acting on the satellite, C_D is the dimensionless drag coefficient, A is the spacecraft area normal to the direction of flight $\mathbf{e_v}$ (unit vector), m is the mass of the spacecraft, ρ is the atmospheric density, and v_r is the satellite's velocity relative to the surrounding atmosphere. C_D and ρ are the parameters that are the major sources of uncertainty when calculating drag [3].

In the past, the C_D was often assumed to be a constant value, an oversimplification that results in significant errors [4, 5]. A more suitable approach that is widely used is estimating the drag coefficient statistically by observing satellite motion over time. In practise, this means estimating either C_D or the ballistic coefficient $B = C_D \frac{A}{m}$ in Eq. 1 in an orbit determination algorithm. A final approach to obtain C_D is physically modelling satellite drag according to aerodynamic drag theory.

✉ Rens van der Zwaard
   rensvanderzwaard@gmail.com; r.k.vanderzwaard@tudelft.nl

Stefano Speretta
s.speretta@tudelft.nl

Christian Siemes
c.siemes@tudelft.nl

Eberhard Gill
e.k.a.gill@tudelft.nl

1   Faculty of Aerospace Engineering, Delft University
    of Technology, Kluyverweg 1, 2629HS Delft,
    The Netherlands

To obtain values for ρ, empirical thermosphere models are commonly used, which are a statistical fit of past density measurements given a parameterised representation of the atmosphere [6]. These are based on a sparse database of historical density measurements. New and accurate density data sets are sought to improve such models, which will, by extension, improve satellite trajectory predictions. Many such density measurements are obtained by tracking the forces acting on satellites using accelerometers and applying a statistical approach to estimate ρ by inversion of Eq. 1 [7]. However, when also considering C_D as a parameter to estimate, the correlation between density and drag coefficient is near unity due to their linear dependence. Thus, it can be expected that significant scale problems are present in the result of both parameters. C_D and ρ are intertwined, and to convincingly determine one based on tracking satellite motion requires the other to be known. For this reason, if the desired result is ρ, statistically determining C_D leads to poor results and physically modelling C_D is the superior choice.

Physically modelling C_D requires considering how the atmosphere interacts with the satellite and how energy and momentum are exchanged between air particles and the satellite surface, which is described by Gas–Surface Interaction (GSI) theory. GSI calculations depend on atmospheric conditions, such as temperature, composition, relative velocity, and satellite characteristics, such as geometry, surface temperature, and material [8]. Even if all these variables would be precisely known, there is no consensus on how the interactions theoretically occur. The leading theories are not fully validated due to limited in-orbit experimental data. A key unknown is the accommodation of the energy of atmospheric particles that collide with the surface, which is represented by the energy accommodation coefficient α.

Using limited experimental data, several theoretical GSI models have been created to approximate α, which have been used to model physical drag coefficients to obtain accurate density data sets (e.g., [9–11]). The drag coefficient is a function of α, so any error in the modelling of α causes errors in C_D. Therefore, the choice of how to model the accommodation coefficient has a considerable impact on the quality of density data sets, which will propagate to thermosphere models that use such data sets as their basis and, by extension, operational satellite orbit predictions. It would be of great value to be able to experimentally validate the predictions made by GSI models to ensure the extent of energy accommodation is modelled correctly.

In the past, attitude manoeuvres of satellites have provided a unique opportunity to do so. These manoeuvrers change the frontal area and drag coefficient of the satellite, but other satellite properties (temperature, material) can be assumed to stay similar. If density observations are sufficiently close in space and time, the change in atmospheric conditions can be assumed to be negligible. Then, only the

spacecraft geometry with respect to the airflow can be a variable, whose effect can be investigated. The first experiment of this kind was conducted using measurements of the CHAMP satellite in 2002, where the same density estimation algorithm was used, whilst the spacecraft flew sideways for half a day [12]. A second experiment was conducted with measurements of a pair of the Swarm satellites in 2014, flying in formation but with attitude differences of 90 degrees around one axis [13]. Both experiments showed that the density observations were consistent only for one specific value of α, whereas other values gave a significant offset between the density observations. This sensitivity stems from the angle of the satellite surfaces with respect to the atmospheric flow, as illustrated in Fig. 1. For the satellite in attitude (a), the atmospheric flow will predominantly hit the satellite surfaces at a very shallow angle, whereas in attitude (b), the angle is much steeper. This difference in the angles results in a different effect of the energy accommodation normal to the surface on the drag coefficient [14].

For the Swarm experiment, it was possible to use this observation to reflect on the choice of accommodation coefficient, which in previous data processing campaigns was configured to $\alpha = 0.93$ or $\alpha = 1.00$. Density was estimated for each satellite flying at different attitudes, using various constant accommodation coefficients, and for a value of $\alpha = 0.85$, the density estimates were observed to match. Unfortunately, the attitude changes were not part of their nominal operations for both missions. They lasted only a few orbits, allowing only the analysis of a short moment in time and a limited set of atmospheric conditions.

In this paper, we intend to build upon the success of these initial experiments with the goal of obtaining more measurements of the energy accommodation coefficient and C_D. In Low Earth Orbit (LEO), a variation in satellite geometry is occasionally used for operational purposes, where this is called "differential drag" [15]. Creating a difference in drag allows a spacecraft to manoeuvre, for example, for collision avoidance [16, 17] or move satellites into desired locations as part of a constellation [18, 19]. Could differential drag
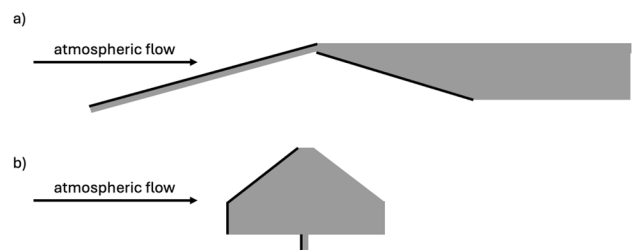
Fig. 1 Attitudes of the Swarm A and Swarm C satellites during the attitude manoeuvre in May 2014, which yielded the highest sensitivity of the density observations to the energy accommodation coefficient. The solid black lines indicate the surfaces most exposed to the atmospheric flow

enable an experiment to estimate the energy accommodation coefficient for a more extended period and, therefore, a more diverse set of conditions? It would be of great value to investigate the dependence of α on atmospheric conditions, as the observed behaviour for energy accommodation could be compared to current GSI theories. An added benefit to estimating α for a mission is that improved drag coefficients could be found for the spacecraft through GSI modelling with proper energy accommodation assumptions, leading to improved orbit predictions and density estimations.

This work attempts to find requirements for such an experiment through extensive simulation. Specifically, it is interesting to see if this could be possible with satellites that do not have accelerometers on board, as only a handful of such missions exist, and attitude manoeuvres are usually not foreseen during their nominal operations. Density estimation based on or assisted by Global Navigation Satellite System (GNSS) measurements has emerged over the last decade [20–23]. Whilst GNSS receivers are not as sensitive as accelerometers, they have proven to be capable hardware for retrieving thermospheric density. Thus, we will use them in this simulation study. GNSS receivers are a typical payload on satellite constellations for navigation purposes. Therefore, if this method proves successful, many experiments could be conducted with hardware already available in abundance in LEO, provided that the mission meets the requirements for the analysis and the required data products can be made available.

In Sect. 2, physical drag coefficient modelling will be explained, as well as the implementation used in this work. Subsequently, the setup will be explained of the simulated satellite mission and experiment. Section 3 starts with a verification of the proposed method, and then presents the results of the simulation study. Section 4 discusses the use and the limitations of the results, leading into a conclusion of the work in Sect. 5.

2 Method

2.1 Drag coefficient modelling

Modelling satellite drag using GSI has been studied, since the moment satellites were in space; insightful reviews about the history and state-of-the-art of orbital aerodynamics are provided by [8, 24, 25]. The objective is to find a representation of the energy and momentum exchange between the atmosphere and the satellite. This exchange is often parameterised using an energy accommodation coefficient α. The definition of the energy accommodation coefficient is the fraction of kinetic energy E that is lost by the interaction between the particle and the satellite surface

$$\alpha = \frac{E_i - E_r}{E_i - E_s}. \tag{2}$$

Here, indices i and r stand for incident and reflected, respectively, and s indicates the energy that the particle carries away from the surface in case a complete thermal accommodation is achieved. In the case of *complete accommodation*, we speak of a *diffuse reflection* ($\alpha = 1$). The case where the particle scatters off the surface and retains its velocity is called a *specular reflection* ($\alpha = 0$). This representation of the interaction between the atmosphere and the surface is an essential input for calculating the drag coefficient.

A widely used model for calculating the drag coefficient is the Diffuse Reflection with Incomplete Accommodation (DRIA) GSI model. The central assumption is that particles are always reflected with a diffuse angular distribution following the cosine law defined by Knudsen [26], but, depending on the energy accommodation coefficient, energy may be exchanged with the surface. The former assumption of diffuse reflection ($\alpha = 1$) was used by Sentman [27] to derive equations to calculate the drag coefficient. At altitudes below 300 kms, this assumption of a nearly complete accommodation is valid, but there is disagreement at higher altitudes [28]. Moe et al. [29] saw the limitation in the assumption of complete accommodation. They derived, based on earlier work [30], a version of Sentman's equations that accounts for a variable accommodation coefficient ($\alpha < 1$), which forms the basis of the DRIA model.

The DRIA GSI model has found success in modelling the drag coefficient to improve consistency with satellite observations [9, 29, 31] and it is used in the Swarm experiment mentioned in the introduction [13], which motivates DRIA as our GSI model of choice in our analysis. More GSI models exist [24, 25] and similar successful results are obtained. The purpose of this work is not to compare GSI models, and alternatives to DRIA are not studied in this work. It is expected that similar results can be obtained using other GSI models. However, different GSI parameters are often used and would need to be estimated, and different models result in different outcomes for the drag coefficients in similar conditions. Therefore, caution should be taken to compare the results of different models with each other [3].

A phenomenon that complicates the calculation of drag coefficients is that atomic oxygen tends to cover parts of the satellite surfaces. This effect is called *adsorption* and affects GSI [32]. Depending on the atmospheric pressure, parts of the surface may be covered with atomic oxygen or not, leaving two regions with different degrees of energy accommodation. To attempt to include the influence of adsorption into GSI models for satellite aerodynamic modelling, the concept of an *adsorption isotherm* is introduced by [33], which is an empirical representation of the coverage of a surface by a gas or fluid

$$\theta = \frac{KP_O}{1 + KP_O}, \tag{3}$$

where θ is a fraction indicating how much of the surface is covered, K is an empirical constant, and P_O is the pressure of atomic oxygen. The fraction θ is a convenient parameter to calculate a total drag coefficient $C_{D,T}$ as a weighted average of the two different regions

$$C_{D,T} = (1 - \theta)C_{D,s} + \theta C_{D,\text{ads}} \tag{4}$$

where $C_{D,ads}$ is the drag coefficient of a surface covered with atomic oxygen and $C_{D,s}$ is the drag coefficient of the clean surface. For the covered surface, we assume complete accommodation $\alpha_{ads} = 1$. For the clean surface, the accommodation coefficient follows Goodman's empirical model [4, 34]:

$$\alpha_s = \frac{K_s \mu}{(1 + \mu)^2}, \tag{5}$$

where $\mu = m_i/m_s$, the ratio between the mass of the incident particle and the mass of the surface material particle, and K_s is a value that depends on the shape of the satellite. Using α_{ads} and α_s as input, $C_{D,ads}$ and $C_{D,s}$ can be calculated, respectively, using DRIA.

For the implementation in this study, it was chosen to use the openly available Response Surface Model (RSM) software package developed by West Virginia University [4, 35]. It can numerically calculate drag coefficients using DRIA

and the adsorption isotherm, of which the implementation in the software is as described in this section. Given a specific satellite geometry and a range of possible atmospheric conditions, the toolkit applies a Test Particle Monte Carlo (TPMC) method to calculate drag for individual gas particles colliding with the satellite. It then builds a regression model of C_D based on independent variables such as atmospheric composition and temperature, and satellite parameters, such as velocity, attitude, and temperature. This regression model can be generated upfront and evaluated for relatively efficient C_D calculations at every time step of an orbit propagation algorithm. A schematic overview of this described workflow is shown in Fig. 2.

2.2 Mission concept

This study is done in preparation for a satellite mission under development, and therefore, we choose to model the satellites according to foreseen mission parameters. The satellites we analyse are a duo of identical spacecraft (A and B) following the PocketQube standard [36], each three units in size (5 cm x 5 cm x 15 cm). The geometry of the two satellites is depicted in Fig. 3. In this simulation, the geometry is kept simple, and any protruding features such as antennae are ignored, as this keeps the computational effort required by the RSM toolkit reasonable.

Two solar panels of 5 cm x 15 cm are deployed, which can be configured at different deflection angles compared to the satellite body. The purpose of the solar panel

Fig. 2 Schematic overview of using the WVU-RSM toolkit to calculate the drag coefficient
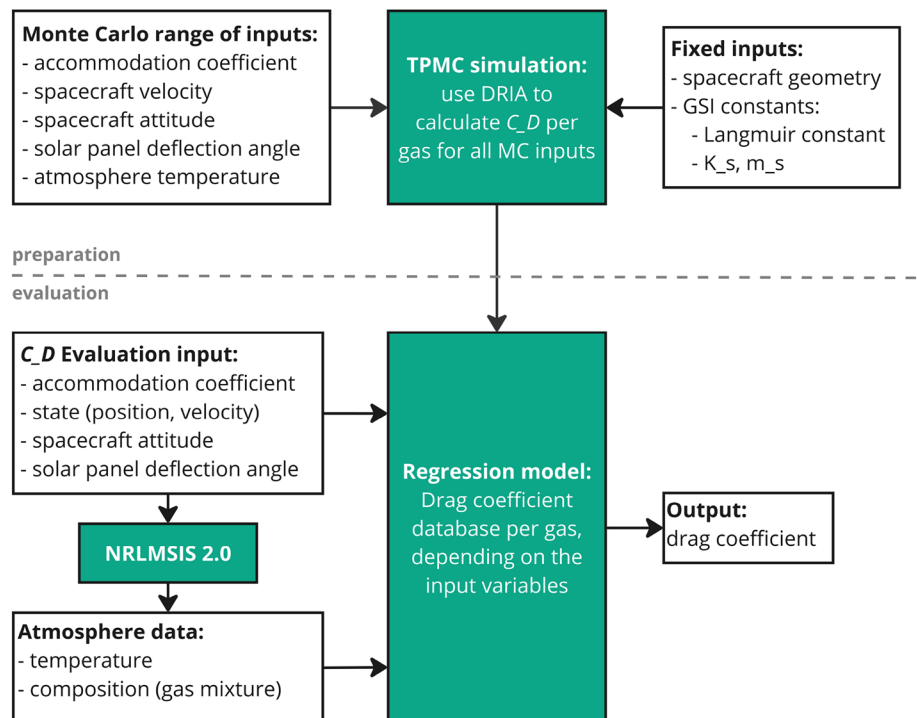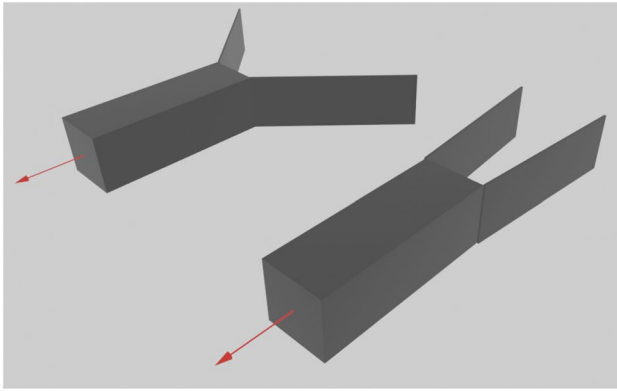
Fig. 3 A simple panel model of the satellite duo simulated in this paper. The satellites are shaped as cuboids with dimensions 15 cm x 5 cm x 5 cm to simplify the aerodynamic and radiation pressure calculations. Two solar panels with dimensions 15 cm x 0.1 cm x 5 cm are attached at the back, and their deflection is defined as the angle with respect to the long side of the body. Satellite A, in the front, has a solar panel deflection of 5°, and satellite B, in the back, has a solar panel deflection of 45°. The satellites fly in the direction of the red arrow, with the solar panels on the backside acting like the feathers of a shuttle, assisting the satellite in keeping a stable attitude
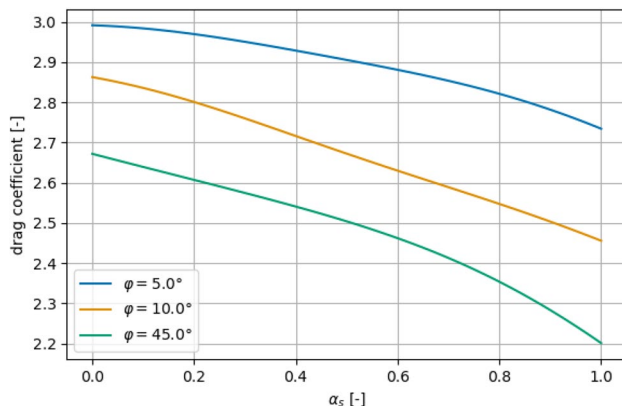
Fig. 4 Dependence of the drag coefficient of the PocketQube at the initial epoch of the orbit indicated in Table 1 on α_s and solar panel deflection angle φ. Calculations are made using the DRIA GSI model using the WVU-RSM toolkit

deflection is to create differential drag between the satellites to manoeuvre them relative to each other without propulsion [37]. Figure 4 gives an example of the behaviour of the drag coefficient based on the solar panel deflection and α_s. Following GSI theory, surfaces that have a shallow angle to the airflow still interact with a significant amount of particles and, therefore, there is a substantial contribution of shear to the total drag. This effect causes C_D to decrease as the solar panel deflection angle increases. Note that C_D behaves in the opposite way to the drag area A, which increases with the panel deflection angle, causing the total drag force to also increase following Eq. 1, as this effect is larger compared to the drag coefficient.

As a baseline, we choose a deflection angle of 5° for satellite A as the solar panels are almost parallel to the flow but the flow still impacts the panel, creating a high drag coefficient. For satellite B we choose 45°, as the drag coefficient is substantially different, but the frontal area of the satellite is still reasonable to prevent a high rate of orbital decay.

Additional mission parameters are given in Table 1. Both satellites start in a sun-synchronous orbit at 400 kms. Satellite B is trailing behind satellite A in-track; this difference is introduced as a separation in the true anomaly in the initial conditions, set to 50 kms of separation. The mission date is chosen as a moment of low solar activity and practically no geomagnetic activity. A point in time in 2019 is selected as space weather and atmospheric density data are readily available. The choice of these parameters is made from foreseen mission parameters, but they do impact the results of the experiment. Therefore, the sensitivity of the results with respect to mission parameters will be discussed in Sect. 3.3.

2.3 Simulation setup

At the top level, the steps taken to run the full simulation experiment are schematically depicted in Fig. 5. First, a satellite mission is simulated, called the "simulated truth" in this paper. The mission parameters, as described in Sect. 2.2, are taken as a starting point, from which satellite orbits are generated. Given certain hardware (i.e., measurement noise) and observation schedules, observations are simulated. We continue as if the simulated observations are obtained using

Table 1 The benchmark mission profile

Mission profile	
Orbit	Sun-Synchronous orbit at 400 km altitude
Mass	600 g
Solar panel deflection	5 degrees for Satellite A 45 degrees for Satellite B
Initial Separation	50 km along-track
Orbit determination arc length	8 h (roughly 5 orbits)
Date	2019-12-01
Space Weather	Low solar activity ($F_{10.7} \approx 70$, $K_p \leq 1$)

Fig. 5 Schematic overview of the simulation setup. OD: Orbit Determination. α_s: energy accommodation coefficient of clean surfaces. ρ_A, ρ_B: estimated density using data of satellite A or B, respectively
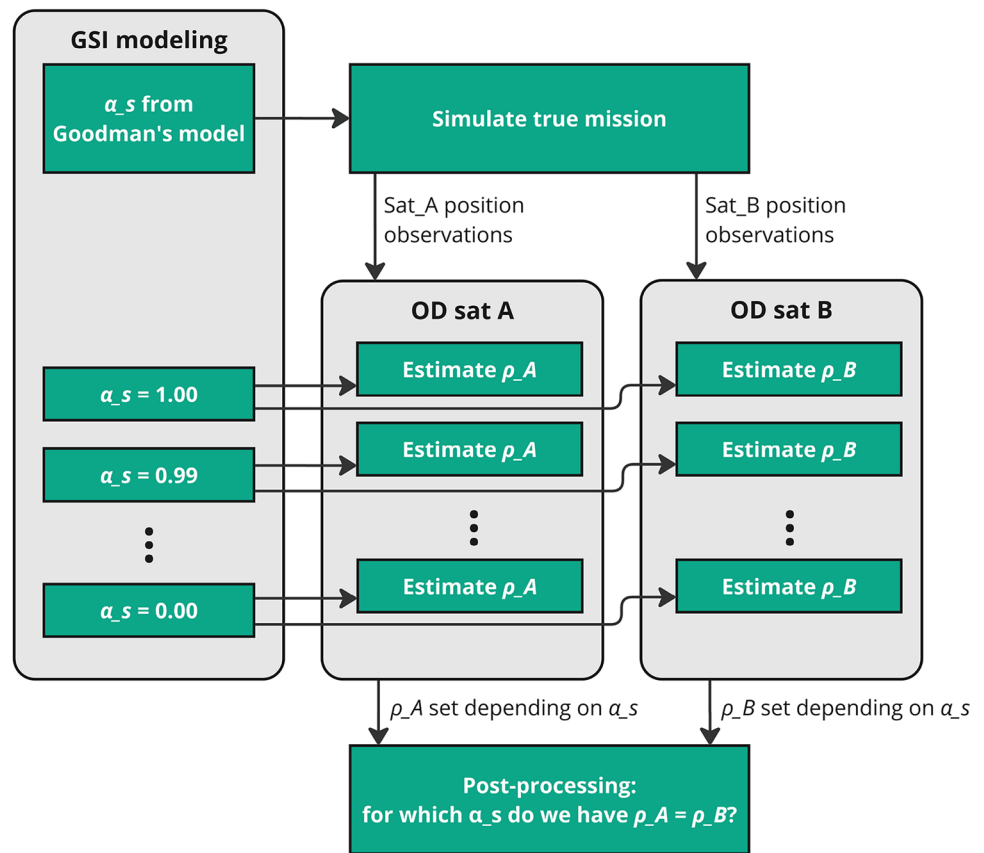
a real mission: we do not know the original orbit and we do not know the density, drag coefficients, or the value used for α_s. The objective of this research is to develop an algorithm that extracts the right value for α_s using satellite observations.

To do so, we utilise an orbit determination algorithm. Unfortunately, because the drag coefficients have to be numerically calculated, directly estimating α_s using orbit determination is not possible. Instead, we pick a constant value for α_s upfront and estimate, for each satellite separately, the initial state and the atmospheric density (more specifically, a scaling factor as a proxy for density is estimated; this will be explained below). The result for estimated density values relies linearly on C_D because of the linear relation of C_D and ρ in the drag calculation (Eq. 1). If C_D values contain errors, the estimated density outcome will be different for both satellites. This is an indication of incorrectly chosen GSI model parameters, because the satellites fly in close proximity, and we can assume they fly through the same atmosphere, so density should be equal. Therefore, the orbit determination process is repeated for a range of constant values for α_s, and we review in post-processing for which α_s we see a match in atmospheric density. As explained in the introduction, the result of previous experiments and the

hypothesis of this research is that there is only one value for α_s where the estimated density will match.

The implementation of all steps was written using TU Delft Astrodynamics Toolbox (Tudat). Its documentation[1] elaborates on many details considering the exact force and environment models that are used in this work. Its core is a non-linear batch least-squares algorithm for orbit determination, which is an implementation of the algorithm described in [2, Chapter 8]. Table 2 provides an overview of the models and parameters used in the benchmark setup; the contents of the table will be elaborated in the remainder of this section.

We assume that information on the satellite attitude is available, although with limited accuracy, and therefore simulate attitude errors using a normal distribution with zero mean and 1-degree standard deviation. The sensitivity analysis in Sect. 3.3 will also discuss systematic attitude errors.

For gravity modelling, a spherical harmonics model is used for the Earth up to degree and order 8. Point mass gravity of the Sun and Moon is included as well. The detail of this gravity model is basic compared with the state-of-the-art in-orbit propagation and determination. However, gravity

---

[1] https://docs.tudat.space/en/latest/

Table 2 Benchmark force and environment models for both the simulated truth and the orbit determination setup

	Simulated truth	Orbit determination
Satellite modelling		
Attitude	As shown in Fig. 3	1-degree error around each axis
Non-aerodynamic force modelling		
Earth gravity	Spherical harmonics up to degree and order 8	Spherical harmonics up to degree and order 8
3rd body gravity	Point mass gravity of Sun and Moon	Point mass gravity of Sun and Moon
Solar Radiation Pressure	Panel model	Panel model, where material emissivity and diffusion contain a 50% error
Aerodynamic force modelling		
Density	HASDM-DB interpolation	NRLMSIS 2.0 with a static scaling factor that is estimated once per arc
Composition and temperature	NRLMSIS 2.0	NRLMSIS 2.0
Horizontal winds	HWM-14	HWM-14 with a 25 m/s error
Drag coefficient	DRIA, α_s calculated using Goodman's model	DRIA, constant α_s
Observations		
Measurement type	3D Position measurements (x, y, z)	
Measurement frequency	every 10 s	
Measurement noise	10 cm	

modelling is not the focus of this study, and it is assumed that in real situations, any uncertainties caused by gravity modelling are negligible compared to other errors, such as radiation and aerodynamic modelling [20, 38].

The solar radiation pressure modelling is done using a simple panel model of the satellites, with fidelity as depicted in Fig. 3. The solar radiation pressure implementation of Tudat is based on [2, Equation 3.72], which calculates the solar radiation pressure for a panel given coefficients of material reflectivity and diffusion. For density estimation algorithms, imperfect radiation pressure modelling is usually a considerable source of error [7], although with arc lengths of multiple orbits, the effect on the density estimation should be minimal. To make the orbit determination realistic, errors are simulated in the solar radiation pressure calculations with respect to the simulated truth. The aforementioned attitude errors are one source of error, but in addition, we assume that the emissivity and diffusion characteristics of the satellite material are poorly known and simulate a 50% error on the coefficients with respect to the simulated truth. These factors together cause random errors with a magnitude of around 10% with respect to the solar radiation pressure accelerations of the simulated truth.

Atmospheric density is a key variable in this study and two sources will be used to retrieve atmospheric density. For density in the simulated truth, we make use of High Accuracy Satellite Drag Model (HASDM) [39, 40], which is a data assimilation system that uses tracking information of dozens of reliable satellites to calibrate the Jacchia-Bowman 2008 (JB2008) empirical density model in near-real time. It is currently the most accurate density model running

in near-real time. Unfortunately, HASDM is not available for public use, but its output up to 2019 is provided for the purpose of scientific research: the HASDM Density Database [41]. The uncertainties of the database are reported to be between 2 and 11% [41], although understanding the accuracy of the database is still an open question [7]. In our implementation, values at specific times and locations are found through multivariate linear interpolation of the database.

In the orbit determination setup, use is made of the Naval Research Labatory Mass Spectrometer, Incoherent Scatter Radar (NRLMSIS) 2.0 [42, 43]. The NRLMSIS series of models are empirical models which are widely adopted in spacecraft operations due to their ease of use. The model does come with limitations: the spatial and temporal resolution is limited [5, 44] and large-scale errors are present due to scale issues in the data sources that the empirical model depends on [6, 45]. In our orbit determination setup, a scale factor on the NRLMSIS 2.0 density output is chosen to be estimated once per arc. This is a proxy for directly estimating a single constant density value per arc. This choice results in lower residuals due to the ability of NRLMSIS 2.0 to provide large-scale density variations along an orbit. Besides density, NRLMSISE 2.0 is able to provide atmospheric composition and temperature, which are used for both the simulated reality and the orbit determination. Composition and temperature are required input for the C_D calculations.

Whilst neither thermosphere model is perfect, we chose to use two independent methods to retrieve densities for the simulated truth and the orbit determination. This ensures that, like in real scenarios, a perfect representation of
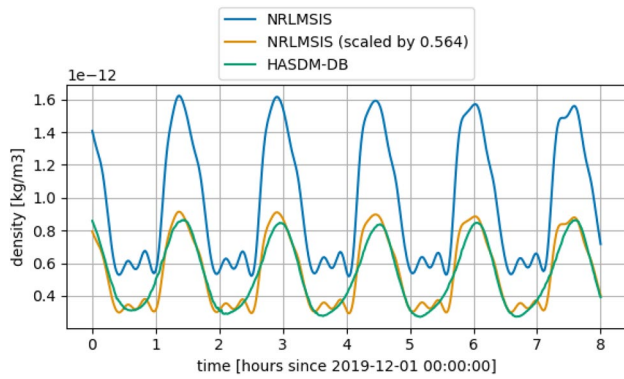
Fig. 6 Thermospheric density over 8 h (roughly 5 sun-synchronous orbits at 400 km altitude), as obtained by interpolating the HASDM Database (green), by evaluating the NRLMSIS 2.0 model (blue), and the NRLMSIS 2.0 output multiplied by a scaling factor which was estimated in an orbit determination run (orange)

thermospheric density cannot be found in the orbit determination process. Figure 6 presents a comparison of the model output for one arc as an example, including an example of the NRLMSIS 2.0 output multiplied by an estimated scale factor in an attempt to approach the HASDM Database output.

Because a scaling factor is not enough to replicate the HASDM densities, high observation residuals would be present in the orbit determination result. Empirical acceleration terms are added to the set of estimated parameters to absorb high residuals. For each orbit, four extra parameters are estimated [2]: two constant acceleration parameters in the along-track direction multiplied by the sine and cosine of the true anomaly, respectively, and two similar terms in the radial direction. The across-track direction is relatively unaffected by the sources of error in this simulation and empirical terms in this direction were not found to be helpful for reducing the residuals.

For simulating winds in the thermosphere, the Horizontal Wind Model (HWM-14) [46] is used in the simulated truth. Like the NRLMSIS models, HWM-14 is an empirical model based on satellite data. It shares its strengths, easy evaluation and the ability to provide a first-order estimate, and shortcomings, low resolution, and errors stemming from its data sources. In our experiment, we can expect to know the climatology of winds by means of a wind model and, therefore, should have a first-order estimate for winds, but should still account for errors in this model. Therefore, we use the output of HWM-14 but simulate an error in both outputs, winds in the meridional and zonal directions. These samples are taken independently for each satellite: wind errors are generated in an uncorrelated manner, taking samples from a normal distribution with zero mean and 25 m/s standard deviation independently for the two satellites. Knowing what standard deviation should be chosen to represent the

uncorrelated error is difficult, but 25 m/s is a representative value for the uncertainty in the HWM-14 model [46]. In Sect. 3.3, the standard deviation is doubled and it turns out the algorithm is relatively insensitive to wind errors. Correlated deviations, i.e., the same wind error is acting on both satellites due to their proximity, are also considered but was not found to have an effect. Both satellites are affected in the same way by such errors, and the result for α_s was found to be unaffected. Vertical winds are smaller in magnitude, to the extent that they are hardly measurable even using accelerometers [47], and therefore neglected.

For observations, 3D position measurements are simulated every 10 s for both satellites, with errors generated using a normal distribution with zero mean and 10 cm standard deviation in each dimension. It is assumed that such measurements can be derived by processing measurements from GNSS receivers onboard both satellites. Such processing is routinely done for space-born GNSS receivers (for example, some recent small satellite missions: [48, 49]). The chosen noise level is a starting point for this study. The sensitivity of the solution to the noise level will be analysed in Sect. 3.2.

Drag coefficients are generated using the WVU-RSM toolkit using the DRIA GSI model. In the simulated truth, the accommodation coefficient α_s is calculated using Goodman's model (Eq. 5). In the orbit determination algorithm, a constant value α_s is chosen, as explained at the beginning of this subsection. Values used in this are $K = 1.44 \cdot 10^6$ in Eq. 3 as found by [28], and $K_s = 3.0$ and $m_s = 3.14 \cdot 10^{-26}$ kg in Eq. 5, all of which are default values in the WVU-RSM toolkit [35]. The mass of the incident particle m_i is an average, dependent on the composition and temperature of the atmosphere. Due to variations of the atmosphere throughout the orbit, the values of α_s and C_D change as well along the arc, as shown in Fig. 7, where the periodic change along the orbital period of approximately 1.5 h can clearly be observed.

Due to the variation of α_s in the simulated truth, we cannot directly compare the orbit determination solution, which uses a constant α_s, to our simulated truth. A reference value has to be determined to define the error of the result. A straightforward choice would be to take the mean of the curve in Fig. 7. However, in past efforts to estimate an effective density or other constant parameters using an extended arc of satellite tracking data, weighing by the amount of drag resulted in a closer representation [50, 51]. We will adopt the drag-weighted mean of the curve of Goodman's model as the desired solution of the α_s in the orbit determination result. It was found that this choice indeed gives a better match compared to simply taking the mean, because it mitigates the influence of partial orbits at the end of the window on the mean. In the arc depicted in Fig. 7, the drag-weighted mean of α_s is approximately 0.005 larger compared
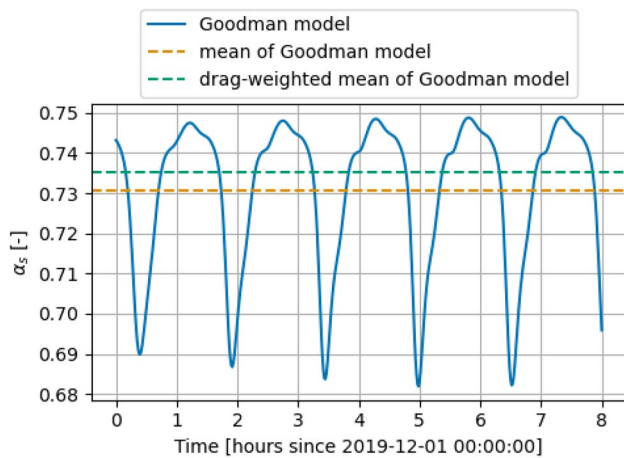
Fig. 7 The variation of α_s as given by Goodman's model (Eq. 5) for satellite A over the course of 8 h (roughly 5 orbits) using the initial conditions described in Table 1. The mean of the curve is indicated with the orange dashed line. The drag-weighted mean is indicated by the green dashed line. Due to the proximity of satellite B with respect to the path length of the orbit, the difference in α_s is negligible between these satellites and would not be visible in Fig.

to a conventional mean, as the larger values for α_s are found in the part of the orbit where drag is larger. Whilst a constant cannot represent a varying parameter, we will refer to the drag-weighted mean as the true solution in analysing the results.

3 Results

3.1 Verification

The goal of this study is to find the accommodation coefficient through density measurements obtained by tracking two formation-flying satellites which are identical except for their aerodynamic configuration. Before looking at results that represent a realistic mission, we aim to verify this method of estimating the accommodation coefficient. To do this, we present a case where the orbit and environment models are identical in the generation of the simulated truth and the orbit determination. This means that, for both cases, the models in the right column of Table 2 are used, with two exceptions: Goodman's model is still used for obtaining α_s in the simulated truth, and the simulated position observations are generated using 1 mm Gaussian noise. This allows us to verify whether our method works in theory in case modelling is done perfectly and with extremely low measurement errors.

The central figure for estimating the accommodation coefficient is Fig. 8. The orbit determination algorithm has been repeated for the same arc using different constant values for α_s, represented on the vertical axis. The resulting estimated
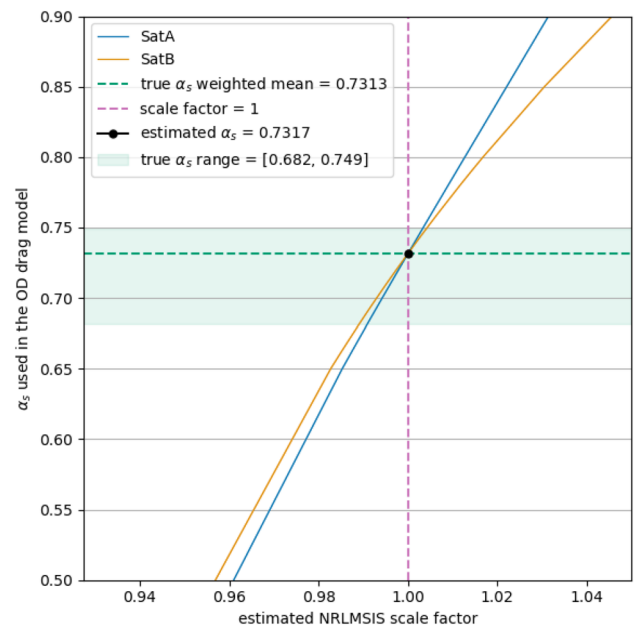
Fig. 8 Orbit determination solutions for an arc of 8 h starting at 2019-12-01 00:00:00 UTC, using the settings described in the first paragraph of Sect. 3.1, for both satellites. The horizontal green line and shaded area are derived from Fig. 7: the dashed green line shows the mean α_s in the simulated reality, and the shaded green area indicates the range of values that α_s has taken on during this arc. The vertical pink dashed line indicates where the estimated scale factor equals 1.00. The blue and orange lines indicate the NRLMSIS scale factor found in orbit determination for satellite A and satellite B, respectively, based on the fixed coefficient α_s that was used as input for the drag modelling. To find an estimated value for α_s, we choose the point where the blue and orange lines cross, indicated with a black dot. For good visibility of the crossing, not the full range of α_s from 0 to 1 is shown, but the blue and orange lines continue to diverge outside the frame and only cross in the domain shown in this figure

NRLMSIS 2.0 scale factors are plotted for both satellites. For most values of α_s, inconsistent drag coefficients are given by the GSI models (as visualised in Fig. 4). The direct consequence is that density is underestimated or overestimated due to their linear dependence in the drag calculation (Eq. 1). The hypothesis of this research is that there is one value for α_s for which the results of both satellites should match, and this value is our solution, as atmospheric density should be equal for both satellites. In this verification run, the correct scale factor is 1, as the density models used in the simulated truth and orbit determination are identical. The value where the lines cross is found through linear interpolation, as the estimation is run for discrete values of α_s in steps of 0.01. In this case, the crossing point is found to be $\alpha_s = 0.7313$, which differs only in the fourth significant digit when compared to the drag-weighted mean of the values in the simulated truth, which is $\alpha_s = 0.7317$.

To further support the algorithm's performance, the estimation was executed for 25 subsequent data arcs. The mean

of the relative difference of the estimated value for α_s with respect to the true solution per arc of the simulated truth is 0.5%, and the maximum offset out of the 25 runs is 1.3% or approximately 0.01.

3.2 Mission scenarios

Our main goal is to show whether the described method to determine the accommodation coefficient is feasible given a representative scenario. Section 2.3 describes the choices that were made to create a representative simulation of a potential mission. The measurement noise was an arbitrary parameter to choose, as this research aims to find a requirement for measurement accuracy of GNSS measurement hardware. It was set to 10 cm as a benchmark, and alternatives will be explored later in this section.

The results are presented similarly as the verification runs in Sect. 3.1. The result of the first run is outlined in Fig. 9. Note that there is no longer a solution for the density scale factor that we can refer to, as the scaled NRLMSIS 2.0 model attempts to approximate the HASDM-DB densities but will never fully match (see Fig. 6). The point where the estimated NRLMSIS scale factors cross now has a visible error with respect to the drag-weighted mean of
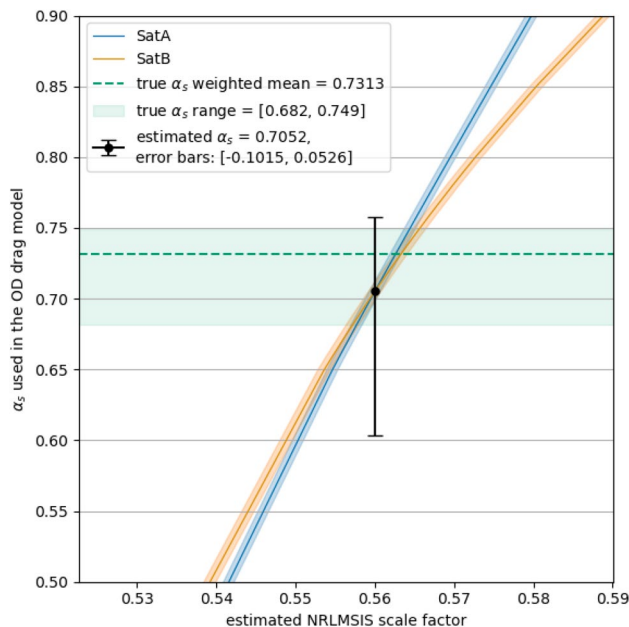
Fig. 9 Orbit determination solutions for an arc of 8 h starting at 2019-12-01 00:00:00 UTC, using the settings described in Sect. 2.3. The meaning of the lines is the same as described in the caption of Fig. 8, with the following additions. Around the blue and orange lines, shaded areas are drawn, indicating the formal uncertainty that the orbit determination attributed to the estimated scale factor. The black error bars are drawn where the edges of the orange and blue shaded areas cross and aim to provide an estimate of uncertainty to accompany the result for α_s

the simulated truth, α_s is underestimated by 0.026, an error of 3.5% relative to the drag-weighted mean. Because the measurement noise is 100 times larger and error sources are present in the force and environment modelling, there is a visible uncertainty associated with the estimates of the density scaling factors, depicted as a shaded area around the blue and orange lines. This uncertainty is the square root of the parameter covariance associated with the estimation and indicates the statistical uncertainty of the batch least-squares algorithm based on the observations [2]. In an attempt to quantify the uncertainty of the estimate of α_s, black error bars are drawn on the locations where the shaded areas cross.

Again, to present a result with statistical relevance, the simulation is repeated for 25 subsequent arcs, as is shown in Fig. 10. The mean absolute offset of the estimation result relative to the true solution is 0.043, or 5.9% with respect to the true solution. There are outliers present, but in the majority of arcs the solution is in the range of values that α_s takes on in the simulated truth, and the true solution is within the error bars associated with the results. The mean uncertainty of the α_s estimates is 10.4%, more pessimistic than the actual offsets, but the variation of α_s along the orbit of the simulated truth can be expected to have an effect on this.

One important parameter that is within the control of the algorithm designer is the arc length, which should be considered carefully. If it is set to be very long, plenty of measurements are available for orbit estimation, but a constant value is fitted to a phenomenon that changes over time, and the constant parameter might not be a good representation. The other side is that too short an arc length means that the satellites have not experienced an amount of differential drag to make the difference measurable within our measurement capabilities. The relation between the drag signal and the measurement noise dictates a minimum arc length, but is difficult to deduce upfront and is not an absolute threshold.

Given this fact, we attempt two different scenarios. The first is a scenario where a satellite is only equipped with a GNSS receiver with limited precision but wishes to conduct this experiment. Figure 11 shows the results of the algorithm when an observation arc of one day is chosen, for a satellite where the position observations have a noise of 25 cm. It can be observed that, even though the arc is three times as long, the algorithm struggles to find an accurate solution for α_s consistently. The mean offset is 11.9% but there are outliers up to 42%. The mean uncertainty derived from the formal errors is 19.5%, a justified drop in confidence.

The second scenario is one where it is desired to estimate the accommodation coefficient once per orbit. If it would be possible to perform accommodation coefficient estimation on a sub-orbital scale instead of just a global scale, information could be derived about the dependency of the accommodation coefficient based on latitude or altitude or on the day–night cycle of the atmosphere. In Fig. 12, the

Fig. 10 Orbit determination solutions for 25 arcs starting at 2019-12-01 00:00:00 UTC, using the settings described in Sect. 2.3. In the upper plot, the light blue line is α_s according to Goodman's model, as used in the simulated reality. The dark blue line represents the drag-weighted mean of α_s in the simulated reality for each arc. Each black dot with error bars represents the orbit determination result of one 8-hour data arc. The first black dot and error bars result from Fig. 9. In the lower plot, a comparison is given between the true and estimated atmospheric density
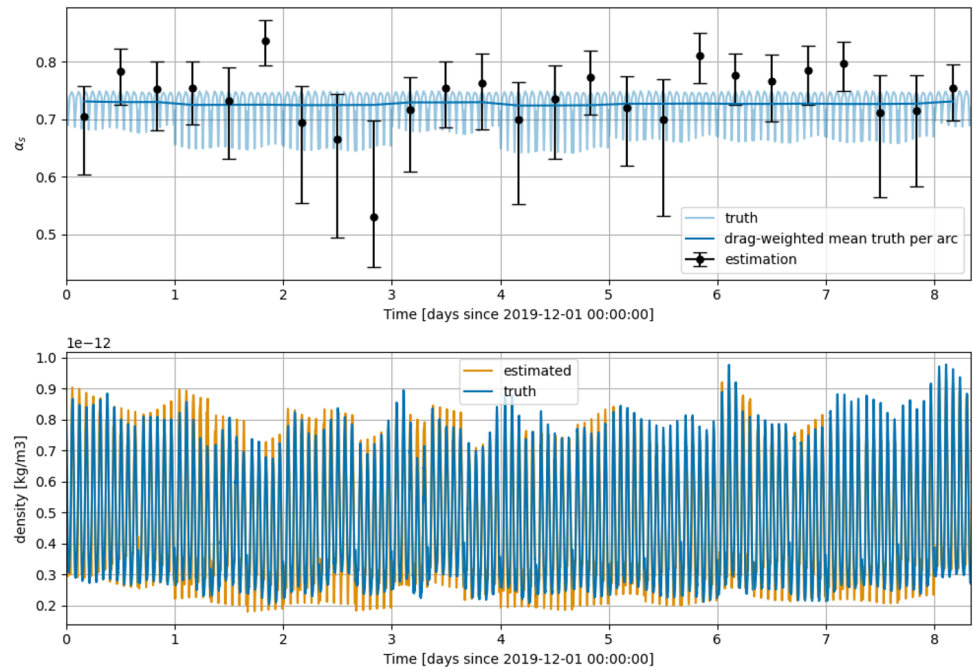
Fig. 11 Orbit determination solutions for 25 arcs starting at 2019-12-01 00:00:00 UTC, using the settings described in Sect. 2.3, except that the POD noise is 25 cm and the arc duration is 24 h. For a detailed description of the lines drawn, see the caption of Fig. 10
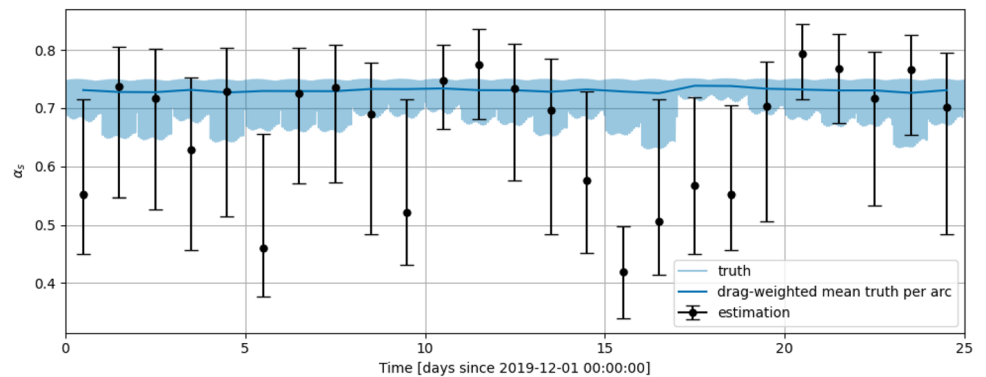
Fig. 12 Orbit determination solutions for 25 arcs starting at 2019-12-01 00:00:00 UTC, using the settings described in Sect. 2.3, except that the POD noise is 1 cm and the arc duration is one orbital period (approximately 93 min). For a detailed description of the lines drawn, see the caption of Fig. 10
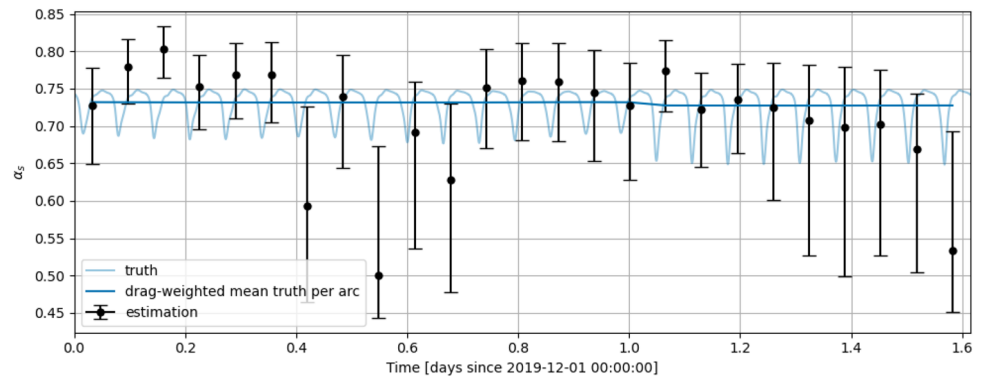
results are shown when the arc duration is one orbit, and the position observations have a noise of 1 cm. However, whilst for many arcs, the estimation is successful, there are also large outliers up to 31%, and 1 cm precision is not sufficient to result in consistent estimations of α_s on an orbital level.

The mean offset is 6.7% and the mean uncertainty of the α_s estimates is 12.3%.

3.3 Sensitivity to mission parameters and model errors

In Sect. 2.3, it was explained that error sources had to be introduced in the modelling choices between the simulated reality and the orbit determination to have a representative simulation. Whilst methods were chosen to be as realistic as possible, they were still arbitrarily chosen. The same holds for the selected mission configuration such as the orbit and the satellite shape. This section aims to show through a sensitivity analysis how the algorithm performs when choices are different.

The setup of Table 2 is taken as a benchmark, for which the results were explained in Sect. 3.2, specifically Fig. 10. The algorithm is run multiple times, changing only one parameter. Checking the sensitivity to many input parameters brings with it a great demand in computational performance. Therefore, we can only touch upon a few different scenarios, and we limit ourselves to reprocessing the first 5 arcs out of 25. Our interest is to show relative changes in the outcome, as the absolute results will be dependent on the mission setup and, therefore, only useful in that specific example.

Two output metrics will be compared: the mean and offset of the estimated accommodation coefficient compared to the true solution and the uncertainty estimate as determined by the estimation algorithm derived from the formal

Table 3 Statistics of α_s estimations after changing one input parameter with respect to the benchmark case, which are the first five arcs of Fig. 10 and follow the setup described in Sect. 2.3. The mean true error is the mean absolute offset of the estimated value for α_s with respect to the drag-weighted average of the simulated truth. The algorithm uncertainty is the mean value of the uncertainty estimates given by the formal uncertainty of the algorithm, as explained in Sect. 3.2. For some arcs this formal uncertainty could not be calculated, generally because the error bars went below $\alpha_s = 0.0$ or above $\alpha_s = 1.0$. In these cases, the algorithm uncertainty is not given in the table

Change	Mean true error		Algorithm uncertainty	
Benchmark	0.053	7.3%	0.064	8.6%
Doubled wind error (50 m/s)	0.054	7.4%	0.065	8.8%
Doubled SRP error (100%)	0.053	7.3%	0.064	8.6%
10-degree random attitude error	0.053	7.3%	0.064	8.6%
10-degree systematic attitude error	0.094	12.9%	0.031	4.0%
Wing deflection satellite B 10 degrees	0.171	23.5%	N/A	N/A
Initial altitude 450 km	0.133	18.9%	0.152	20.5%
Initial altitude 500 km	0.248	36.8%	N/A	N/A
Satellite mass halved (300 g)	0.025	3.5%	0.031	4.3%
Satellite mass doubled (1200 g)	0.097	13.3%	0.131	17.3%
100 km initial separation	0.060	8.2%	0.053	6.9%
500 km initial separation	0.239	32.9%	N/A	N/A

uncertainties of the density estimations. The results are given in Table 3.

The setup is insensitive to doubling wind errors and solar radiation model errors. For the latter, even unfeasible errors (over 100% of nominal values) were tested, and the same effect was found. This insensitivity is a consequence of radiation pressure being substantially smaller than drag at the benchmark's altitude of 400 km. For random attitude errors, i.e., measurement errors in pitch and yaw are simulated with zero mean and 10-degree standard deviation, the outcome for α is similarly unchanged. This can be explained by the observation arcs lasting multiple orbits, which causes errors to average out, and due to the ability of the empirical acceleration terms to absorb these effects. For example, the solar radiation pressure errors have a periodic nature and are fully absorbed by the empirical acceleration terms. A systematic attitude error, i.e. both satellites have an independent 10-degree bias in a random direction in yaw and pitch, causes a significant increase in error. It causes a bias in the estimated density, because C_D and A are scaled in a systematic way, corrupting the estimation of the correct density.

The impact of mission design changes is also given. A run was performed where satellite B has a wing deflection of 10 degrees instead of 45 degrees, which is much closer to the 5 degrees deflection of satellite A. The impact is that the drag coefficients are closer together (see Fig. 4) causing the density estimates to be closer together. Visually, this means that in Figs. 8 and 9, the blue and orange lines are closer together (with identical panel deflections, the drag coefficients would be equal, and the blue and orange lines would be identical). The crossing of the lines happens at an increasingly shallow angle and determining the exact crossing point will be more prone to errors.

Increasing the altitude of the satellites means decreasing the atmospheric density and, subsequently, drag acting on the satellite, making the effects on the orbit less visible and difficult to distinguish from the noise in position measurements. High errors in α_s are the result at altitudes of 450 km and 500 km. Considering that the simulation was done at low solar activity, the possibility of estimating α_s can be stretched to higher altitudes for periods of medium or high solar activity. Similar to the GNSS measurement noise level, it would make sense to consider the choice of arc length of the estimation based on the altitude, as it is a driving factor for the magnitude of the density and drag force.

Similarly, the satellite mass was halved and doubled to assess the effect of a changing ballistic coefficient. The amount of drag inversely scales with satellite mass, and therefore, errors decrease as mass decreases. Here it should be noted that satellites of the PocketQube standard have a high relative mass-to-frontal area ratio compared to most other satellites, due to the need of packing the required hardware into a small volume with little free space. It is therefore

a conservative experiment, and the algorithm will perform better for satellites which have a higher area-to-mass ratio, for example, CubeSats or satellites with more surfaces normal to the airflow such as solar panels.

Increasing the separation between the satellites affects the assumption that both satellites fly through the same atmosphere. If a density value was directly estimated, this would have an impact, as the (average) density will be different for both satellites. Because we estimate a scaling factor on the NRLMSIS 2.0 output, and this factor is global instead of for local parts of the atmosphere, the effect of the distance between the satellites is somewhat mitigated. However, besides density, also α_s is a parameter determined by atmospheric parameters and changes along the orbit (Fig. 7). The true α_s becomes different for both satellites due to their different orbits, complicating the estimation of a single constant coefficient. This is a shortcoming of estimating constant parameters for phenomena that change with location, which seems to be a valid choice for our formation-flying mission. An estimation setup could account for local differences in its parameter estimation setup using atmosphere models, which we would recommend for satellites not flying in close formation. Also, one should note that the close formation is lost over time during differential drag operations, increasing the distance between satellites. To account for this, in the suggested mission analysed in this paper, the satellites would alternate between each other with their panel deflections after an observation arc, which will make the satellites approach each other again [37]. This also helps to keep the relative orbital decay in check for both satellites.

4 Discussion

This research aimed to simulate a possible experiment to estimate the extent of energy accommodation and characterise the requirements of such an experiment. It is shown through verification in Sect. 3.1 that, theoretically, the algorithm will find a representative value for α_s in the case of perfect modelling and observations with 1 mm noise; the solution is consistent with the values used in the simulated truth within 1%.

Next, results were generated for missions with GNSS receivers that provide a position observable with precision in the order of decimetres. GNSS receivers with this capability are increasingly common onboard satellites for navigation purposes. Satellites with a scientific objective that requires precise positioning are usually also in the centimetre to decimetre range. In Sect. 3.2, estimates for α_s are done using three different position noise levels. For centimetre level GNSS noise and higher, it is shown that estimates could be found on a scale of hours to days, and

a precision in the order of 5–10% should be expected. This precision serves as an indicative measure and should be used carefully, as it is derived from just 25 simulated data arcs due to constraints in computational resources.

The various cases in this study mainly aim to show the relative impact of the GNSS receiver precision. Several other mission parameters, such as altitude, inter-satellite separation, and ballistic coefficient, have a visible impact on the results due to their effect on the drag force. It indicates that the arc duration has to be tuned according to the drag signal and GNSS measurement noise of the analysed mission, and the temporal resolution and precision of the estimates for α_s are given accordingly. In addition, mission design parameters such as the ballistic coefficient could be tuned to improve a possible experiment. This observed relation between signal, noise, and arc duration is analogous to experiences in estimating thermospheric density, where global estimates can be found with most GNSS receivers and sub-orbital resolution can only be achieved with science-grade GNSS receivers or accelerometers [7].

In terms of force and environment modelling in the orbit determination setup, it is observed that random errors in attitude or wind and systematic errors in solar radiation modelling have negligible effects on the benchmark mission, mainly due to the long arc durations and empirical estimation terms included in the orbit determination. These effects could become larger for shorter arcs and more precise accommodation coefficient estimation. A prominent increase in estimation errors is found when systematic errors are present in the attitude determination, as this introduces a bias in the drag coefficient and frontal area in calculating atmospheric drag. This indicates that attitude determination free of systematic errors is a clear requirement to perform such an experiment.

One limitation is the choice of DRIA as a GSI model and the specific implementation including the isotherm, limiting this study to that method only. The choice of implementations dictates how C_D depends on the energy accommodation coefficient, and therefore affects the estimation results. Similarly, in an actual experiment, the solution statistically found using tracking data will depend on the assumption of GSI models in the orbit determination model [33]. Suppose one is interested in using the resulting accommodation coefficients or drag coefficients of such an estimation; it is essential to use GSI models consistently in predictions, as it is common for different GSI models to predict different drag coefficients based on the energy accommodation [4]. More so, with sufficient experimental data, it might become possible to compare different GSI models against each other to study how models compare in their agreement with the measurements.

5 Conclusion

The origin of this research lies in the fact that there is a lack of experiments to characterise satellite drag, resulting in limited knowledge on how to calculate the drag coefficient C_D. Errors in C_D propagate to errors in satellite orbit predictions. Atmospheric density estimations performed through orbit determination are affected by drag coefficient errors, and these errors will propagate to empirical thermosphere models that rely on such data.

This study aims to demonstrate that one mission characteristic, differential drag, can be exploited to create an experiment. By measuring the impact of atmospheric drag on satellites for different aerodynamic configurations, α_s can be singled out as a variable that affects the drag exerted on the satellite. It can be estimated using the data from this experiment, solving for an important unknown parameter in the calculation of C_D.

The mission simulation performed in this paper considered two identical PocketQubes flying in formation at an altitude of 400 km, where varying solar panel deflections created differential drag. Position observations were generated with a precision of decimetres, a capability that is increasingly common on small satellites for navigation purposes. It was demonstrated that the proposed algorithm functions correctly and that on a time scale of hours to days, the accommodation coefficient can be estimated with an error in the order of 5–10%. Considering the scarcity of in-orbit experiments, such results could be a useful result in thermospheric drag research [3, 8, 13].

This paper shows a limited case study and results are specific to the simulated mission. However, its intention is to present that satellite missions with differential drag, GNSS receivers, and attitude determination and control can contribute to the open area of research on atmospheric drag. The example shown is two formation-flying satellites, however, no reason can be identified why this setup could not work on a more diverse set of missions. For example, a satellite constellation distributed over a larger area or a single satellite changing attitudes periodically could yield similar results, if one properly considers these factors during data processing. It is presumed that missions already performing differential drag operations can satisfy these requirements (e.g., [18, 19]). The drag signal and precision on the GNSS receiver dictate the temporal frequency and accuracy at which the accommodation coefficient can be estimated. In addition, performing such an experiment can lead to drag coefficients and thermospheric density estimates that are relatively free of bias, which are highly desired products both in satellite operations and research.

Declarations

Competing interests The authors declare no competing interests.

References

1. Hejduk, M.D., Snow, D.E.: The effect of neutral density estimation errors on satellite conjunction serious event rates. Space Weather **16**(7), 849–869 (2018). https://doi.org/10.1029/2017SW001720

2. Montenbruck, O., Gill, E.: Satellite Orbits: Models, Methods and Applications, 1st edn. Springer, Berlin (2000)

3. Bruinsma, S., Wit, T., Fuller-Rowell, T., Garcia-Sage, K., Mehta, P., Schiemenz, F., Shprits, Y.Y., Vasile, R., Yue, J., Elvidge, S.: Thermosphere and satellite drag. Adv. Space Res. (2023). https://doi.org/10.1016/J.ASR.2023.05.011

4. Mehta, P.M., Walker, A., McLaughlin, C.A., Koller, J.: Comparing physical drag coefficients computed using different gas-surface interaction models. J. Spacecr. Rocket. **51**(3), 873–883 (2014). https://doi.org/10.2514/1.A32566

5. Vallado, D.A., Finkleman, D.: A critical assessment of satellite drag and atmospheric density modeling. Acta Astronaut. **95**(1), 141–165 (2014). https://doi.org/10.1016/j.actaastro.2013.10.005

6. Emmert, J.T.: Thermospheric mass density: a review. Adv. Space Res. **56**(5), 773–824 (2015). https://doi.org/10.1016/j.asr.2015.05.038

7. Bruinsma, S., Siemes, C., Emmert, J.T., Mlynczak, M.G.: Description and comparison of 21st century thermosphere data. Adv. Space Res. (2022). https://doi.org/10.1016/J.ASR.2022.09.038

8. Mehta, P.M., Paul, S.N., Crisp, N.H., Sheridan, P.L., Siemes, C., March, G., Bruinsma, S.: Satellite drag coefficient modeling for

thermosphere science and mission operations. Adv. Space Res. (2022). https://doi.org/10.1016/j.asr.2022.05.064

9. March, G., Visser, T., Visser, P.N.A.M., Doornbos, E.N.: CHAMP and GOCE thermospheric wind characterization with improved gas-surface interactions modelling. Adv. Space Res. **64**(6), 1225–1242 (2019). https://doi.org/10.1016/j.asr.2019.06.023

10. Mehta, P.M., Linares, R.: A methodology for reduced order modeling and calibration of the upper atmosphere. Space Weather **15**(10), 1270–1287 (2017). https://doi.org/10.1002/2017SW001642

11. Pilinski, M.D., Argrow, B.M., Palo, S.E.: Semiempirical model for satellite energy-accommodation coefficients. J. Spacecr. Rocket. **47**(6), 951–956 (2010). https://doi.org/10.2514/1.49330

12. Doornbos, E.: Thermospheric density and wind determination from satellite dynamics. PhD thesis, Delft University of Technology (2011). https://doi.org/10.1007/978-3-642-25129-0

13. March, G., Van Den Ijssel, J., Siemes, C., Visser, P.N.A.M., Doornbos, E.N., Pilinski, M.: Gas-surface interactions modelling influence on satellite aerodynamics and thermosphere mass density. J Space Weather Space Climate (2021). https://doi.org/10.1051/swsc/2021035

14. Bernstein, V., Pilinski, M.: Drag coefficient constraints for space weather observations in the upper thermosphere. Space Weather (2022). https://doi.org/10.1029/2021sw002977

15. Traub, C., Romano, F., Binder, T., Boxberger, A., Herdrich, G.H., Fasoulas, S., Roberts, P.C.E., Smith, K., Edmondson, S., Haigh, S., Crisp, N.H., Oiko, V.T.A., Lyons, R., Worrall, S.D., Livadiotti, S., Becedas, J., González, G., Dominguez, R.M., González, D., Ghizoni, L., Jungnell, V., Bay, K., Morsbøl, J., Garcia-Almiñana, D., Rodriguez-Donaire, S., Sureda, M., Kataria, D., Outlaw, R., Villain, R., Perez, J.S., Conte, A., Belkouchi, B., Schwalber, A., Heißerer, B.: On the exploitation of differential aerodynamic lift and drag as a means to control satellite formation flight. CEAS Space J **12**(1), 15–32 (2020). https://doi.org/10.1007/s12567-019-00254-y

16. Gaglio, E., Traub, C., Turco, F., Murcia Piñeros, J.O., Bevilacqua, R., Fasoulas, S.: Optimal drag-based collision avoidance: balancing miss distance and orbital decay. Acta Astronaut. **228**, 295–305 (2025). https://doi.org/10.1016/j.actaastro.2024.11.052

17. Omar, S.R., Bevilacqua, R.: Spacecraft collision avoidance using aerodynamic drag. J. Guid. Control. Dyn. **43**(3), 567–573 (2020). https://doi.org/10.2514/1.G004518

18. Foster, C., Mason, J., Vittaldev, V., Leung, L., Beukelaers, V., Stepan, L., Zimmerman, R.: Constellation phasing with differential drag on planet labs satellites. J. Spacecr. Rocket. **55**(2), 473–483 (2018). https://doi.org/10.2514/1.A33927

19. Kumar, B.S., Ng, A., Yoshihara, K., De Ruiter, A.: Differential drag as a means of spacecraft formation control. IEEE Trans. Aerosp. Electron. Syst. **47**(2), 1125–1135 (2011). https://doi.org/10.1109/TAES.2011.5751247

20. IJssel, J., Doornbos, E., Iorfida, E., March, G., Siemes, C., Montenbruck, O.: Thermosphere densities derived from Swarm GPS observations. Adv. Space Res. **65**(7), 1758–1771 (2020). https://doi.org/10.1016/j.asr.2020.01.004

21. Calabia, A., Jin, S.: Thermospheric density estimation and responses to the March 2013 geomagnetic storm from GRACE GPS-determined precise orbits. J. Atmos. Solar Terr. Phys. **154**, 167–179 (2017). https://doi.org/10.1016/j.jastp.2016.12.011

22. Sutton, E.K., Thayer, J.P., Pilinski, M.D., Mutschler, S.M., Berger, T.E., Nguyen, V., Masters, D.: Toward accurate physics-based specifications of neutral density using GNSS-enabled small satellites. Space Weather (2021). https://doi.org/10.1029/2021SW002736

23. Wöske, F., Huckfeldt, M., Rievers, B.: Tailored accelerometer calibration by POD for thermospheric density retrieval with GRACE and GRACE-FO. Adv. Space Res. **74**(10), 4517–4542 (2024). https://doi.org/10.1016/j.asr.2024.09.021

24. Livadiotti, S., Crisp, N.H., Roberts, P.C.E., Worrall, S.D., Oiko, V.T.A., Edmondson, S., Haigh, S.J., Huyton, C., Smith, K.L., Sinpetru, L.A., Holmes, B.E.A., Becedas, J., Domínguez, R.M., Cañas, V., Christensen, S., Mølgaard, A., Nielsen, J., Bisgaard, M., Chan, Y.A., Herdrich, G.H., Romano, F., Fasoulas, S., Traub, C., Garcia-Almiñana, D., Rodriguez-Donaire, S., Sureda, M., Kataria, D., Belkouchi, B., Conte, A., Perez, J.S., Villain, R., Outlaw, R.: A review of gas-surface interaction models for orbital aerodynamics applications. Prog. Aerosp. Sci. **119**, 100675 (2020). https://doi.org/10.1016/J.PAEROSCI.2020.100675

25. Mostaza, P.D., Graziano, B.P., Roberts, P.C.E.: Spacecraft drag modelling. Elsevier Ltd (2014)

26. Knudsen, M.: Das Cosinusgesetz in der kinetischen Gastheorie. Ann. Phys. **353**(24), 1113–1121 (1916). https://doi.org/10.1002/andp.19163532409

27. Sentman, L.H.: Free molecule flow theory and its application to the determination of aerodynamic forces. Technical report (1961). https://apps.dtic.mil/sti/tr/pdf/AD0265409.pdf

28. Walker, A., Mehta, P., Koller, J.: Different implementations of diffuse reflection with incomplete accommodation for drag coefficient modeling. J. Spacecr. Rocket. **51**(5), 1522–1532 (2014). https://doi.org/10.2514/1.A32668/ASSET/IMAGES/LARGE/FIGURE14.JPEG

29. Moe, K., Moe, M.M., Rice, C.J.: Simultaneous analysis of multi-instrument satellite measurements of atmospheric density. J. Spacecr. Rocket. **41**(5), 849–853 (2004). https://doi.org/10.2514/1.2090

30. Schamberg, R.: A New Analytic Representation of Surface Interaction for Hyperthermal Free-molecule Flow, with Application to Satellite Drag. RAND Corporation, Santa Monica, California (1958)

31. Sutton, E.K.: Normalized Force Coefficients for Satellites with Elongated Shapes. J. Spacecr. Rocket. **46**(1), 112–116 (2009). https://doi.org/10.2514/1.40940

32. Moe, K., Moe, M.M., Wallace, S.D.: Improved satellite drag coefficient calculations from orbital measurements of energy accommodation. J. Spacecr. Rocket. **35**(3), 266–272 (1998). https://doi.org/10.2514/2.3350

33. Walker, A., Mehta, P., Koller, J.: Drag coefficient model using the Cercignani-Lampis-Lord gas-surface interaction model. J. Spacecr. Rocket. **51**(5), 1544–1563 (2014). https://doi.org/10.2514/1.A32677/

34. Goodman, F.O., Wachman, H.Y.: Formula for thermal accommodation coefficients. J. Chem. Phys. **46**(6), 2376–2386 (1967). https://doi.org/10.1063/1.1841046

35. Sheridan, P.L., Paul, S.N., Avendaño-Franco, G., Mehta, P.M.: Updates and improvements to the satellite drag coefficient Response Surface Modeling toolkit. Adv. Space Res. **69**(10), 3828–3846 (2022). https://doi.org/10.1016/j.asr.2022.02.044

36. TU Delft, Alba Orbital, GAUSS Srl.: The PocketQube Standard (Issue 1.0). Technical report (2018)

37. Centrella, M.: Mission and system design of a formation-flying picosatellites cluster: a technology demonstration mission for space situational awareness improvement (2023). https://webthesis.biblio.polito.it/28975/

38. Siemes, C., Ijssel, J., Visser, P.: Uncertainty of thermosphere mass density observations derived from accelerometer and GNSS tracking data. Adv. Space Res. **73**(10), 5043–5063 (2024). https://doi.org/10.1016/j.asr.2024.02.057

39. Storz, M.F., Bowman, B.R., Branson, J.I., Casali, S.J., Tobiska, W.K.: High accuracy satellite drag model (HASDM). Adv. Space Res. **36**(12), 2497–2505 (2005). https://doi.org/10.1016/j.asr.2004.02.020

40. Storz, M.F.: HASDM validation tool using energy dissipation rates. In: AIAA/AAS Astrodynamics Specialist Conference and Exhibit. American Institute of Aeronautics and Astronautics Inc., Monterey, California (2002). https://doi.org/10.2514/6.2002-4889

41. Tobiska, W.K., Bowman, B.R., Bouwer, S.D., Cruz, A., Wahl, K., Pilinski, M.D., Mehta, P.M., Licata, R.J.: The SET HASDM density database. Space Weather (2021). https://doi.org/10.1029/2020SW002682

42. Emmert, J.T., Drob, D.P., Picone, J.M., Siskind, D.E., Jones, M., Mlynczak, M.G., Bernath, P.F., Chu, X., Doornbos, E., Funke, B., Goncharenko, L.P., Hervig, M.E., Schwartz, M.J., Sheese, P.E., Vargas, F., Williams, B.P., Yuan, T.: NRLMSIS 2.0: a whole-atmosphere empirical model of temperature and neutral species densities. Earth Space Sci (2021). https://doi.org/10.1029/2020EA001321

43. Picone, J.M., Hedin, A.E., Drob, D.P., Aikin, A.C.: NRLM-SISE-00 empirical model of the atmosphere: Statistical comparisons and scientific issues. J. Geophys. Res. Space Physics 107(A12), 15–1 (2002). https://doi.org/10.1029/2002JA009430

44. Liu, H., Thayer, J., Zhang, Y., Lee, W.K.: The non-storm time corrugated upper thermosphere: what is beyond MSIS? Space Weather 15(6), 746–760 (2017). https://doi.org/10.1002/2017SW001618

45. Bruinsma, S., Sutton, E., Solomon, S.C., Fuller-Rowell, T., Fedrizzi, M.: Space weather modeling capabilities assessment: neutral density for orbit determination at low earth orbit. Space Weather 16(11), 1806–1816 (2018). https://doi.org/10.1029/2018SW002027

46. Drob, D.P., Emmert, J.T., Meriwether, J.W., Makela, J.J., Doornbos, E., Conde, M., Hernandez, G., Noto, J., Zawdie, K.A., McDonald, S.E., Huba, J.D., Klenzing, J.H.: An update to the horizontal wind model (HWM): the quiet time thermosphere. Earth Space Sci 2, 301–319 (2015). https://doi.org/10.1002/2014EA000089

47. Visser, T., March, G., Doornbos, E., Visser, C., Visser, P.: Horizontal and vertical thermospheric cross-wind from GOCE linear and angular accelerations. Adv. Space Res. 63(10), 3139–3153 (2019). https://doi.org/10.1016/J.ASR.2019.01.030

48. Arnold, D., Peter, H., Mao, X., Miller, A., Jäggi, A.: Precise orbit determination of Spire nano satellites. Adv. Space Res. 72(11), 5030–5046 (2023). https://doi.org/10.1016/J.ASR.2023.10.012

49. Conrad, A., Axelrad, P., Zuffada, C., Haines, B., O'Brien, A., Loria, E.: Improved orbit determination of the CYGNSS satellites and its application to GNSS-R ocean altimetry. International Geoscience and Remote Sensing Symposium (IGARSS), 5847–5850 (2020) https://doi.org/10.1109/IGARSS39084.2020.9323760

50. Picone, J.M., Emmert, J.T., Lean, J.L.: Thermospheric densities derived from spacecraft orbits: accurate processing of two-line element sets. J. Geophys. Res. Space Phys 110(A3), 3301 (2005). https://doi.org/10.1029/2004JA010585

51. Emmert, J.T.: A long-term data set of globally averaged thermospheric total mass density. J. Geophys. Res. Space Physics 114(A6), 6315 (2009). https://doi.org/10.1029/2009JA014102

52. Delft high performance computing centre (DHPC): delft blue supercomputer (Phase 2) (2024). https://www.tudelft.nl/dhpc/ark:/44463/DelftBluePhase2